ROMANIAN JOURNAL OF INFORMATION SCIENCE AND TECHNOLOGY
Volume 28, Number 2, 2025, 125–137
doi: 10.59277/ROMJIST.2025.2.01

Measurement of Electromagnetic Feedthrough in Spin Wave Based Microwave Multiport Devices

Alina-Cristina BUNEA[1], Florin CIUBOTARU[2], Fanfan MENG[2], Christoph ADELMANN[2], Ovidiu-George PROFIRESCU[3], and Dan NECULOIU[2,3,*]

[1]National Institute of R&D in Microtechnologies (IMT), 077190 Bucharest, Romania
[2]IMEC, 3001 Leuven, Belgium
[3]National University for Science and Technology POLITEHNICA Bucharest, 060042 Bucharest, Romania
Email: alina.bunea@imt.ro, florin.ciubotaru@imec.be, fanfan.meng@imec.be, christoph.adelmann@imec.be, profirescu.ovidiu@gmail.com, dan.neculoiu@imt.ro*
* Corresponding author

Abstract. Multiport radio-frequency (RF) input devices are designed to handle multiple signals simultaneously. These devices typically consist of multiple input ports that can receive different RF signals and combine them into a single output or distribute them to multiple outputs. For example, in wave computing, majority gates use an odd number of inputs and one output. This paper investigates the electromagnetic feedthrough of a 3-input/1-output majority gate layout based on spin waves (SWMGs) and U-shaped microwave spin-wave transducers. The paper addresses the challenges of electromagnetic feedthrough by exploring shielding techniques to understand and improve the performance of the SWMG. As a tradeoff in complexity and performance, the unshielded layout is optimized and fabricated on a 500 nm Yttrium Iron Garnet (YIG) film. Measurements of scattering (S-) parameters demonstrate spin wave propagation at 8 GHz for a 200 mT magnetic bias field, with reduced electromagnetic coupling. Furthermore, the study includes an analysis of the effective permittivity and loss tangent of Gadolinium Gallium Garnet (GGG) substrate, critical for accurate electromagnetic modeling of the device.

Key-words: GGG; majority gate; S-parameters; spin wave; YIG.

1. Introduction

Multiport spin wave devices have significant potential for various RF applications, particularly in fields where high-speed, low-power signal processing are essential. Incorporating mul-

tiport spin wave devices into RF applications such as phase-shifting, modulation/demodulation, or RF signal processing could enable more energy efficient, faster solutions compared to conventional RF approaches [1]–[5]. Furthermore, spin-wave (SW) devices for information processing are of considerable interest for further improvement of energy-efficient and cost-effective technologies [6]–[8]. However, the development of functionally meaningful computing systems based on interactions between localized spin waves is not straightforward, and its exploration is still in the stage of infancy [7]. One of the fundamental computing functionalities is provided by majority gates, which have many applications in the design of adders, parity checkers, parity generators, error-correcting codes, and are building blocks for designing complex systems such as decoders and comparators [9], [10].

1.1. Spin wave inductive transducers

Spin waves can be generated by resonant electromagnetic excitation with their properties tailored by material parameters, bias fields and coupling structure design. The time-varying magnetic component of the electromagnetic field exerts a torque on the spins, perturbing their equilibrium alignment and initiating precessional motion. This drives spin waves when the excitation frequency matches the system's resonant modes.

Inductive antennas are microwave spin wave transducers that convert microwave signals into spin waves in magnetic materials, enabling the manipulation of spintronic devices. In this case the RF current flowing in the metal wire creates a magnetic field in the magnetic material that generates spin waves. Several types of inductive spin-wave transducers exist, each with its own advantages and disadvantages (Fig.1).

Wire inductive transducers are the simplest, consisting of a straight wire or microstrip line placed over a magnetic material. Their main advantages are simplicity in design and ease of fabrication, as well as the ability to integrate with existing microelectronic circuits. However, their

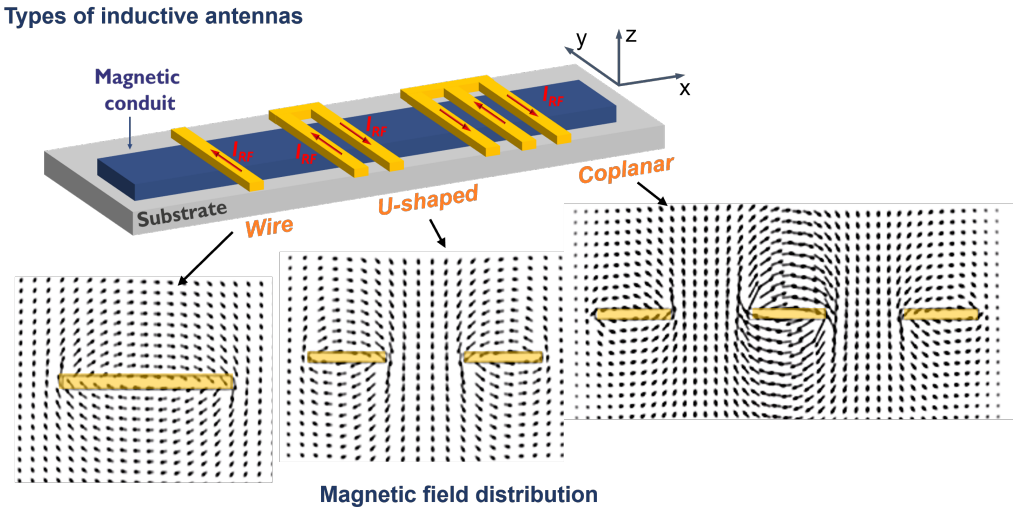

Fig. 1. Types of spin-wave inductive antennas and their magnetic field distributions in the xz-plane created by RF currents with polarities indicated by the red arrows.

efficiency in converting microwave energy to spin waves is limited, and they exhibit narrower bandwidth compared to more complex designs.

U-shaped inductive transducers feature a U-shaped structure, often implemented in microstrip or coplanar circuit topologies, placed over the magnetic material. These transducers provide improved spin wave coupling due to their geometry, allowing for more efficient energy focusing into the spin wave modes.

Coplanar inductive transducers, which employ a coplanar waveguide (CPW) where both the signal and ground conductors lie in the same plane, offer superior impedance matching and lower loss. They also provide better coupling with the magnetic material, particularly in thin film systems. While wire transducers are simple but less efficient, U-shaped transducers improve coupling and energy focus, and coplanar transducers offer the best performance but at the cost of increased complexity and area. Moreover, in the latter case, the non-reciprocal propagation of the spin waves in magnetic thin films like YIG can make the design more difficult. Detection is often the converse process of generation. The same antenna used to launch spin waves (via microwave currents) can detect them by measuring induced voltages from spin-wave-driven magnetic fields.

1.2. Spin wave majority gate overview

Spin wave majority gates (SWMGs) offer a promising alternative to conventional charge-based electronics for logic operations, due to their capability to provide more powerful logic operations (e.g, “AND”, “OR”) in the same device. These devices potentially enable smaller, faster, and more energy-efficient computing systems. They leverage the wave-like nature of electron spin, rather than charge transport, to perform computations. A majority gate consists of an odd number of inputs (larger or equal to 3) and an output whose logic state is ’1’ if the majority of its inputs are set to ’1’, and ’0’ otherwise.

SWMGs typically employ magnetic waveguides that control the spin wave propagation and their interference and transducers for generation/detection. There are two main approaches. The first one is **interference-based SWMGs** [11]–[12]. These designs rely on the constructive and destructive interference of spin waves. Input spin waves are injected into the structure, where they interact. The output is determined by the phase and amplitude of the resulting spin wave at the output port. The output signal intensity determines the logic state. The second approach is based on **non-linear magnetization-dynamics**. [13]–[15]. High-power spin waves are injected, and the nonlinear interactions lead to the generation of new frequencies or changes in the spin wave spectrum. The output logic state is then determined by detecting these changes. This approach can offer higher operating frequencies but faces challenges in controlling nonlinear effects.

Materials employed for the fabrication of SWMGs include **magnetic insulators** such as Yttrium Iron Garnet (YIG), which is widely utilized due to its low magnetic damping, allowing for long-distance spin wave propagation [11]. **Ferromagnetic metals** like permalloy (NiFe) and CoFeB alloys are also used, especially for structures requiring stronger spin wave excitation [12]. These can be integrated with YIG or other magnetic insulators. Emerging research is also exploring **antiferromagnetic materials**, which offer the potential for even faster spin wave propagation and smaller device sizes due to their higher spin wave frequencies. [16]–[17] Materials like Gadolinium Gallium Garnet (GGG) are often used as substrates for YIG, while Silicon is widely used as a substrate for ferromagnetic metals.

While SWMGs are still largely in the research phase, some potential applications have emerged. For example, **beyond-CMOS logic** promises that SWMGs could complement CMOS transistors

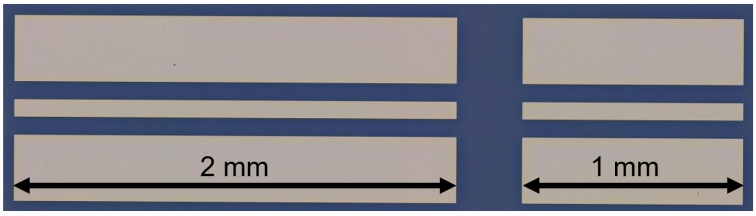

Fig. 2. Photo of the fabricated CPW transmission lines.

in future logic circuits, offering advantages in power consumption and speed [7]. SWMGs are key components for more complex **magnonic devices**, such as spin wave routers, multiplexers, and processors. The ability of SWMGs to perform weighted summation and thresholding operations makes them attractive for **neuromorphic computing** applications [18]–[19].

The current paper addresses the direct electromagnetic feedthrough in an interference-based SWMG topology consisting of U-shaped antennas.

2. GGG Material Parameter Extraction at Microwave Frequencies

Gadolinium Gallium Garnet (GGG) material parameters provided by manufacturers (relative permittivity 30, loss tangent 0.15) differ significantly from reported GHz range measurements. Previous research [20] found a relative permittivity of 11.9 and loss tangent of 0.052 (8.2-12.4 GHz). To address this discrepancy, [21] extracted the effective permittivity of GGG from measured scattering (S)-parameters. Coplanar waveguide transmission lines (CPW-TLs) were fabricated on a 500 µm thick GGG substrate with a 200 nm gold layer. Two CPW-TLs of 1 mm and 2 mm lengths were used (Fig. 2). The CPW-TL has the width of the signal strip of 0.08 mm and the space to ground metalization of 0.08 mm (the line characteristic impedance is close to 50 ohm).

A CS-5 calibration substrate providing standards fit for 150 µm pitch ground-signal-ground (G-S-G) probes was used to perform on-wafer short-open-load-thru (SOLT) calibration, with 1 kHz intermediate frequency (IF). A 2-port Anritsu 37397D vector network analyser (VNA) was used in the experiment.

S-parameters were measured in the 2–55 GHz range, and the effective permittivity was extracted using (1) – (5). The effective permittivity is a fundamental parameter for modeling of planar transmission lines with mixed dielectric layers using a simple homogeneous medium model. It depends on the geometry of the line and permittivities of the surrounding materials and it is crucial for determining parameters like phase velocity, characteristic impedance and wavelength in the line.

$$\gamma = \frac{1}{\Delta L}\operatorname{arctanh}\left(\frac{S_{11}^{B}S_{22}^{A} + S_{11}^{A}S_{22}^{B} - \Delta_A - \Delta_B}{2S_{21}^{B}S_{12}^{A}}\right) \tag{1}$$

$$\Delta L = L_B - L_A \tag{2}$$

$$\Delta_A = S_{11}^{A}S_{22}^{A} - S_{21}^{A}S_{12}^{A} \tag{3}$$

$$\Delta_B = S_{11}^B S_{22}^B - S_{21}^B S_{12}^B \tag{4}$$

$$\varepsilon_{eff} = \frac{\mathrm{Im}(\gamma)^2}{\omega^2 \mu_0 \varepsilon_0} \tag{5}$$

Using a 3D electromagnetic (EM) model (Fig.3) and data fitting, a relative permittivity of approximately 13 and a loss tangent of 0.15 were estimated for the GGG substrate. The comparison of effective permittivity of GGG extracted from measured S-Parameters and simulated results is presented in Fig.4. The agreement is good up to 18 GHz and the model for the GGG material parameters needs improvements for higher frequencies.

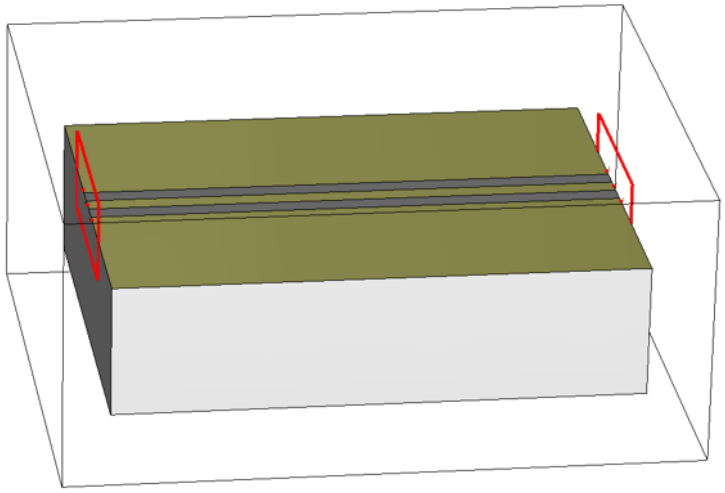

Fig. 3. 3D electromagnetic model of a 2 mm CPW-TL.

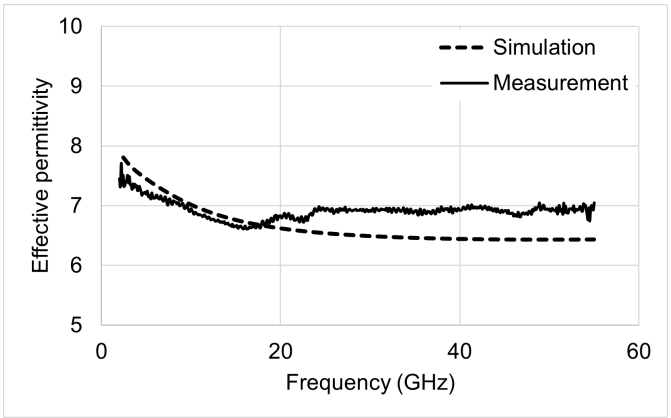

Fig. 4. Comparison of effective permittivity of GGG extracted from measured S-Parameters and electromagnetic simulated results.

3. Investigation of Electromagnetic Feedthrough in a 3-input SWMG Layout with U-shaped Inductive Antennas

A 3-input SWMG layout is designed using U-shaped inductive antennas with the layout configuration from Fig. 5 (a). The metal-gap-metal of the U is 2-2-2 micron. This design achieves peak excitation efficiency when generating spin waves with a 10-micron wavelength. The antennas are connected by 500 micron long coplanar waveguide transmission lines with the configuration from Section 2. Fig. 5 (b) shows a depiction of the three spin waves generated by transducers I1, I2, I3 and their interference at the output (O4).

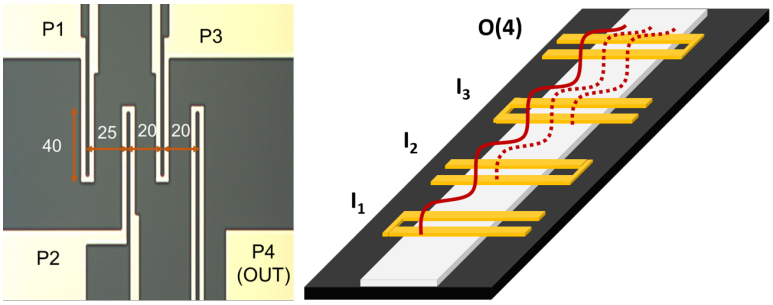

Fig. 5. (a) Layout of a 3-input SWMG with U-shaped transducers (the metallization is yellow; dimensions in microns); (b) representation of the three spin waves generated by transducers I1, I2, I3 and their interference at the output (O4).

Since the inductive antennas are placed close together and the distance between contact pads is very small, an analysis of the direct electromagnetic coupling between the different ports is required. Furthermore, adding a shielding metal connected to the ground plane of the CPW between the transducers is also investigated. Starting from the initial layout from Fig. 6(a), additional metallic isolation structures were placed between the antennas (with green in Fig.

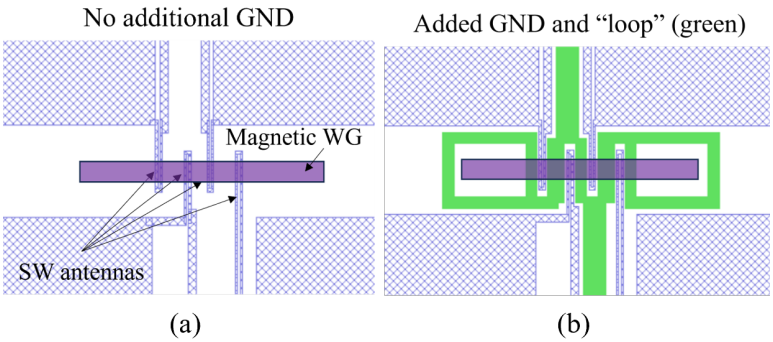

Fig. 6. SWMG layout versions: (a) no additional shielding between the inductive antennas;(b) additional GND strip and loop (green).

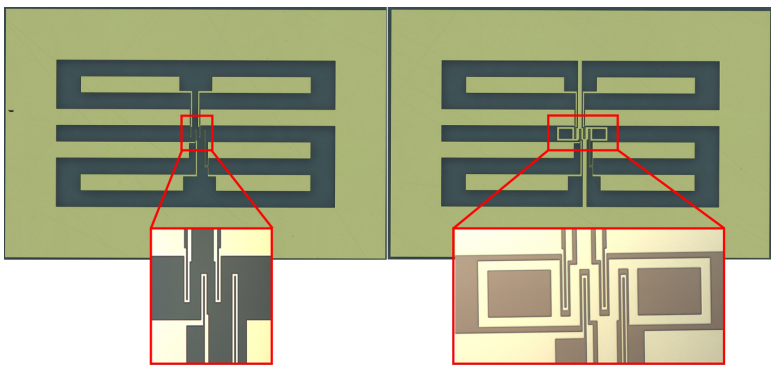

(a) (b)

Fig. 7. Microscope images of fabricated devices: (a) layout without additional shielding between the inductive antennas (inset detail); (b) layout with metal shielding between the inductive antennas (inset detail).

6(b)). Compared to [21] these shielding structures have the shape of loops, in an effort to limit the effect on a magnetic waveguide (purple strip in Fig. 6) placed under the inductive antennas. The distance between the shielding metal and the U-shaped transducers is 2 microns, with a 6 micron gap at the end of the U. The width of the loop metal outside the transducer area is 10 microns.

Test devices used for the assessment of the electromagnetic feedthrough were fabricated on GGG without magnetic material and were characterized by means of on wafer scattering (S-) parameter measurements. Fig. 7 shows photos of the fabricated devices under test.

A on-wafer short-open-load-thru calibration was performed in the 2 - 12 GHz frequency range with 1 kHz intermediary frequency (IF) and 1 MHz frequency step. A 2-port Anritsu ShockLine MS46122A vector network analyzer (VNA) was used in the experiment. The measured 2-port transmission parameters for all port combinations are shown in Fig. 8 for the two layout configurations.

A simplified 3D electromagnetic model was developed in CST Microwave Studio, including

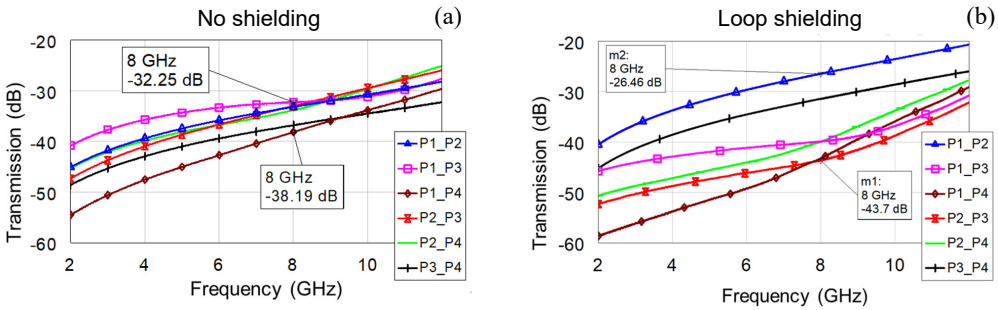

Fig. 8. Transmission parameters for all port combinations: (a) SWMG layout without shielding; (b) SWMG layout with loop shielding.

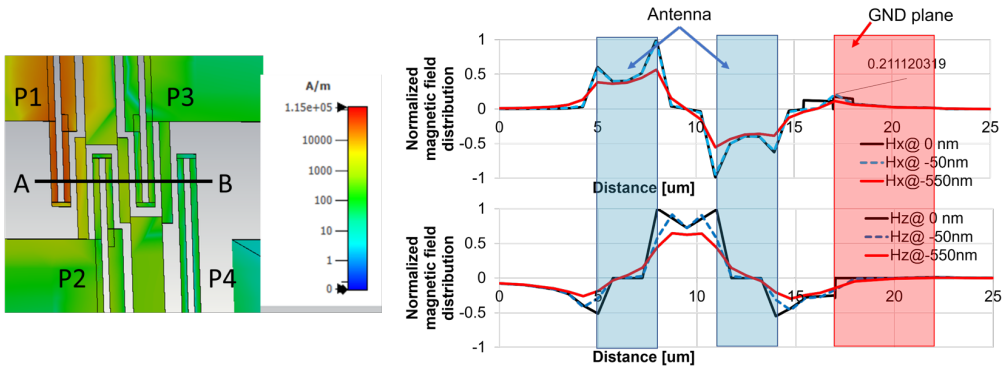

(a) (b)

Fig. 9. (a) Magnetic field magnitude generated by a flowing microwave current in the inductive U-shaped antenna P1. (b) Normalized Hx- and Hz-components of the magnetic field extracted along the black line AB in (a) for different distances beneath antenna surfaces.

only the shielding strips in between the U-shaped antennas. The simulated magnetic field distribution, for an excitation at P1, shows that the current flowing in the shielding (GND) strips placed between the inductive antennas (Fig. 9 (a)), is around 20% of the maximum current flowing through the antennas. The normalized Hx- and Hz-components of the magnetic field extracted along the 'AB'- line from Fig. 9 (a) for different distances beneath the antenna surface is shown in Fig. 9 (b). The current induced in the adjacent GND strip (indicated with red in Fig. 9 (b)) is significant at the edge of the metal, for depths of a few hundred nanometers. It is worth noting that these currents will induce magnetic fields that will generate additional SWs. The interaction with these parasitic SWs would then lead to a degradation of the signal.

The layout without additional ground loops and strips has lower overall risks, such as higher fabrication yield and no potential parasitic SW generation by currents flowing in the shielding metal. Overall, the electromagnetic direct coupling of the no-shielding layout varies within -54 dB and -40 dB at 2 GHz, and between -32 dB and -26 dB at 12 GHz for all port combinations. The layout with a metal shield demonstrated a stronger direct coupling at high frequency, up to -19 dB for the ports P1 and P2 at 12 GHz. Nevertheless, the direct coupling is significantly reduced at low frequency (e.g., at 2 GHz is within -59 dB and -40 dB for all ports). It is obvious that for applications the spin wave signal should be above the direct electromagnetic coupling. The no-shield gives the best trade-off between complexity, risks, and RF performance, and a version of it is fabricated on magnetic material in the next section. These results are in agreement with those presented in [21].

4. SWMG Layout Fabricated on YIG

The layout without shielding from Section 3 was slightly modified by adding tapered transitions from the U-shaped transducers to the coplanar waveguide transmission lines (CPW-TL) used to contact the SWMG ports. This increases the distance between the pads and improves the matching between the U-shaped transducers and input CPW-TLs.

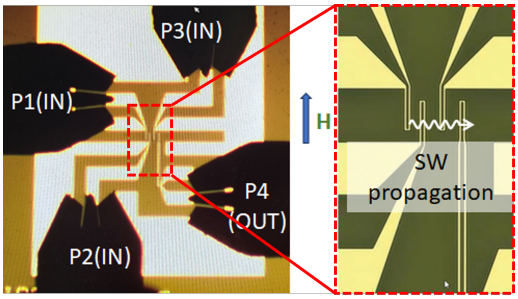

Fig. 10. Microscope image of a SWMG fabricated on YIG: (left) device under test; (right) detail of the transducers with SW propagation direction and magnetic field (H) direction indication.

The devices were fabricated on a 500 nm thick YIG film grown on the GGG substrate. A 50 nm SiO2 was deposited as a protective layer, followed by 250 nm thick Au contacts. A microscope image of a fabricated device under test is shown in Fig. 10 (left), whereas the U-shaped transducers, SW propagation direction and magnetic field (H) orientation can be seen in Fig. 10 (right).

The SWMG test device was characterized by means of on-wafer S-parameter measurements under external magnetic field bias conditions. The setup consists of a Cascade probing station and an electromagnet (Fig. 11).

The two pole extensions of the electromagnet ensure a relatively uniform in-plane magnetic field whose magnitude and polarity depends on the applied current. The SWMG chip was diced (6 mm x 4 mm) to fit in-between the two poles, as shown in Fig. 11. The probes were then connected to a 4-port PNA-X Network Analyzer from Keysight (model N5247B). A on-wafer short-open-load-thru (SOLT) calibration was performed, with intermediate frequency IF=1kHz and frequency step of 1 MHz, and an applied power from VNA of -15 dBm.

Fig. 12 summarizes the behavior of the SWMG device for a magnetic field of 200 mT applied parallel with respect to the U-shaped antennas (see Fig. 10), the so-called Damon-Eshbach geometry, where the spin waves propagate perpendicular to the external field. The ferromagnetic

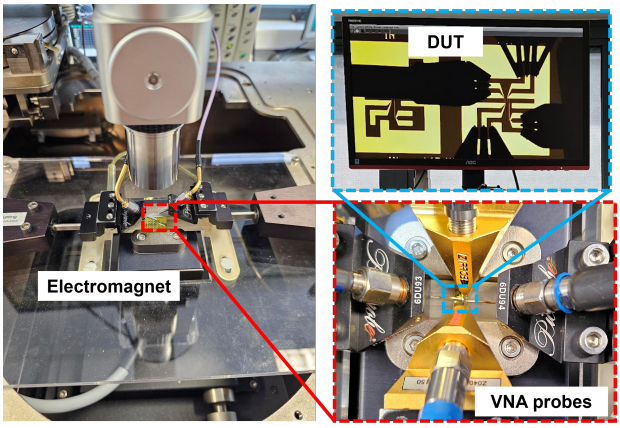

Fig. 11. On-wafer 4-port S-parameter measurement setup.

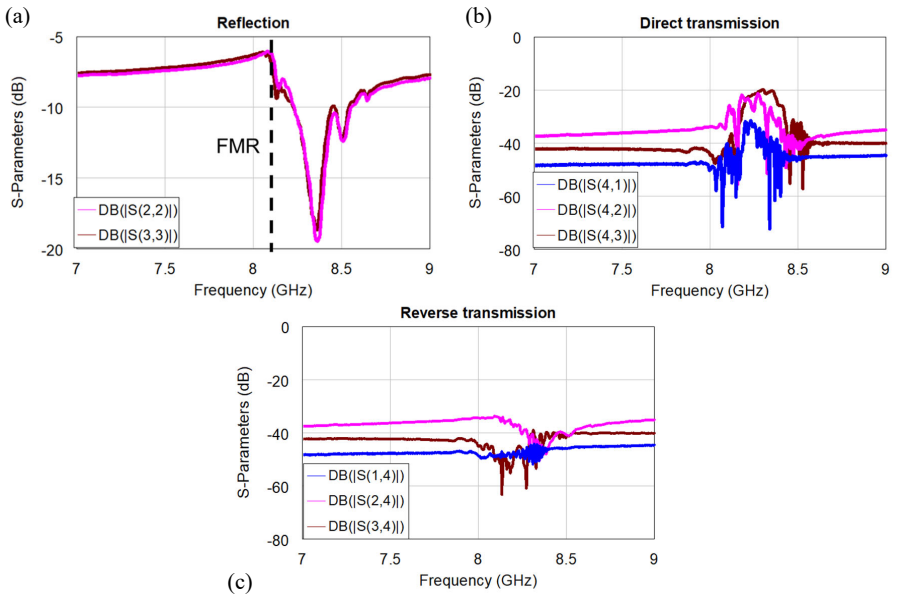

Fig. 12. S-parameter measurement results for a 200 mT magnetic biasing field: (a) reflection parameters for the three input ports; (b) transmission parameters from the three input ports to the output port; (c) reverse transmission from the output port to the three input ports

resonance frequency (FMR) of the YIG film is about 8.1 GHz, and can be determined experimentally considering the start of the absorption band (see Fig. 12 (a)). The FMR is strictly related to the geometrical and magnetic parameters of YIG, hence no difference is observed (as expected) in the reflection parameters for the ports P2 and P3, although they have a mirror symmetry in the device layout.

The transmission (insertion losses) between the three inputs (P1, P2, P3) to the output (P4), where one of the inputs is sweeping and the other two act as 50 Ohm loads is shown in Fig. 12 (b). The maximum transmission is around –31 dB between P1 and P4 (longest propagation distance for spin waves, 65 µm), –21 dB between P2 and P4 (40 µm spin wave propagation distance), and –20 dB for P3–P4 (20 µm spin wave propagation distance). The spin-wave propagation bandwidth band is about 500 MHz centered at 8.35 GHz.

The direct electromagnetic coupling (feedthrough) to the output port around 7.3 GHz (near the spin-wave band) is –48 dB for P1; –36 dB for P2; and –42 dB for P3. The slightly stronger coupling observed between P2 and P4 is due to the longer overlap of the transducers. Nevertheless, if we compare these results to the direct coupling shown in Fig. 8 (a) we notice a clear improvement of up to 10 dB for the new layout, which introduced a tapered design for the U-shaped antenna contacts.

It is worth noting that the spin waves propagation in the Damon-Eshbach geometry are affected by non-reciprocity, i.e., they propagate differently in opposite directions within a magnetic material as a result of excitation efficiency that is orientation dependent [22]–[23]. This can be clearly seen by comparing for example the transmission traces S(4,1) and S(1,4) displayed in Fig. 12(b) and (c). From Fig. 12(c) it is evident that the reversed transmission from P4 to P1,

P2, and P3 for the spin wave band is at or below the level of direct electromagnetic coupling. This suggests that nearly no spin waves are propagating from P4 towards P1, demonstrating the strong asymmetry in the excitation efficiency of spin waves propagating in opposite directions.

It is important to mention that the optimal spin-wave excitation-detection efficiency is reached when the antenna impedance is matched to the spin-wave's radiation resistance through careful antenna design. [24]–[26].

5. Conclusions

In conclusion, this study provides valuable insights into the design and reduction of the direct feedthrough for spin-wave majority gate layouts using U-shaped microwave spin-wave transducers. The analysis of Gadolinium Gallium Garnet (GGG) material parameters and the investigation of direct coupling in multi-port spin wave devices represent a step forward towards mitigating unwanted electromagnetic interference to improve transmitted signal quality. The final layout fabricated on 500 nm Yttrium Iron Garnet (YIG) film showed a measured feedthrough between the input and the output ports of the device in a range of –37…–47 dB for frequencies near the spin wave propagation band, centered around 8.35 GHz, with a bandwidth of 500 MHz. The paper underlines the importance of material properties, transducer design, and shielding techniques in lowering direct electromagnetic feedthrough. As the field of magnonics continues to evolve, multiport spin wave devices offer promising prospects for energy-efficient, high-speed microwave applications. Future work will focus on refining the design for better performance, integrating with existing microelectronic systems, and exploring additional material options to further enhance spin-wave propagation.

Acknowledgement. The authors would like to acknowledge the support of the European Union Horizon Europe research and innovation program under grant agreement no. 101070417 (SPIDER). A.B. also acknowledges the support of the MCID, CNCS/CCCDI - UEFISCDI, project number PN-IV-P8-8.1-PRE-HE-ORG-2023-0042. For the purpose of Open Access the authors have applied a CC-BY public copyright license to any Author Accepted Manuscript version arising from this submission.

References

[1] M. KRAWCZYK and D. GRUNDLER, *Review and prospects of magnonic crystals and devices with reprogrammable band structure*, Journal of Physics: Condensed Matter, **26**, 2014, paper 123202.

[2] A. V. CHUMAK, V. I. VASYUCHKA, A. A. SERGA and B. HILLEBRANDS, *Magnon spintronics*, Nature Physics, **11**(6), 2015, pp. 453–461.

[3] M. COCCONCELLI, S. TACCHI, R. ERDÉLYI, F. MASPERO, A. Del GIACCO, A. PLAZA, O. KOPLAK, A. CATTONI, R. SILVANI, M. MADAMI, Á. PAPP, G. CSABA, F. KOHL, B. HEINZ, P. PIRRO and R. BERTACCO, *Tuning magnonic devices with on-chip permanent micromagnets*, Physical Review Applied, **22**, 2024, paper 064063.

[4] O. L. KHRYSTYNA, K. DAVÍDKOVÁ, J. MIKKELSEN and A. V. CHUMAK, *Review on spin-wave RF applications*, Accessed: Mar. 1, 2025. [Online]. Available: https://arxiv.org/abs/2411.19212.

[5] M. COCCONCELLI, F. MASPERO, A. MICELLI, A. TONIATO, A. DEL GIACCO, N. PELLIZZI, A. E. PLAZA, A. CATTONI, M. MADAMI, R. SILVANI, A. HAMADEH, C. ADELMANN, P. PIRRO, S. TACCHI, F. CIUBOTARU and R. BERTACCO, *Self biased integrated magnonic device*, Accessed: Mar. 1, 2025. [Online]. Available: https://doi.org/10.48550/arXiv.2502.03186.

[6] Z. GUO, J. YIN, Y. BAI, D. ZHU, K. SHI, G. WANG, K. CAO and W. ZHAO, *Spintronics for energy- efficient computing: an overview and outlook*, Proceedings of the IEEE, textbf109(8), 2021, pp. 1398–1417.

[7] A. V. CHUMAK, P. KABOS, M. WU, C. ABERT, C. ADELMANN, A. O. ADEYEYE, J. ÅKERMAN, F. G. ALIEV, A. ANANE, A. AWAD, C. H. BACK, A. BARMAN, G. E. W. BAUER, M. BECHERER, E. N. BEGININ, V. A. S. V. BITTENCOURT, Y. M. BLANTER, P. BORTOLOTTI, I. BOVENTER, D. A. BOZHKO, S. A. BUNYAEV, J. J. CARMIGGELT, R. R. CHEENIKUNDIL, F. CIUBOTARU, S. COTOFANA, G. CSABA, O. V. DOBROVOLSKIY, C. DUBS, M. ELYASI, K. G. FRIPP, H. FULARA, I. A. GOLOVCHANSKIY, C. GONZALEZ-BALLESTERO, P. GRACZYK, D. GRUNDLER, P. GRUSZECKI, G. GUBBIOTTI, K. GUSLIENKO, A. HALDAR, S. HAMDIOUI, R. HERTEL, B. HILLEBRANDS, T. HIOKI, A. HOUSHANG, C.-M. HU, H. HUEBL, M. HUTH, E. IACOCCA, M. B. JUNGFLEISCH, G. N. KAKAZEI, A. KHITUN, R. KHYMYN, T. KIKKAWA, M. KLÄUI, O. KLEIN, J. W. KŁOS, S. KNAUER, S. KORALTAN, M. KOSTYLEV, M. KRAWCZYK, I. N. KRIVOROTOV, V. V. KRUGLYAK, D. LACHANCE-QUIRION, S. LADAK, R. LEBRUN, Y. LI, M. LINDNER, R. MACÊDO, S. MAYR, G. A. MELKOV, S. MIESZCZAK, Y. NAKAMURA, H. T. NEMBACH, A. A. NIKITIN, S. A. NIKITOV, V. NOVOSAD, J. A. OTÁLORA, Y. OTANI, A. PAPP, B. PIGEAU, P. PIRRO, W. POROD, F. PORRATI, H. QIN, B. RANA, T. REIMANN, F. RIENTE, O. ROMERO-ISART, A. ROSS, A. V. SADOVNIKOV, A. R. SAFIN, E. SAITOH, G. SCHMIDT, H. SCHULTHEISS, K. SCHULTHEISS, A. A. SERGA, S. SHARMA, J. M. SHAW, D. SUESS, O. SURZHENKO, K. SZULC, T. TANIGUCHI, M. URBÁNEK, K. USAMI, A. B. USTINOV, T. VAN DER SAR, S. VAN DIJKEN, V. I. VASYUCHKA, R. VERBA, S. VIOLA KUSMINSKIY, Q. WANG, M. WEIDES, M. WEILER, S. WINTZ, S. P. WOLSKI and X. ZHANG, *Advances in magnetics roadmap on spin-wave computing*, IEEE Transactions on Magnetics, **58**(6), 2022, pp. 1–72, paper 0800172.

[8] A. MAHMOUD, F. CIUBOTARU, F. VANDERVEKEN, A. V. CHUMAK, S. HAMDIOUI, C. ADELMANN and S. COTOFANA, *Introduction to spin wave computing*, Journal of Applied Physics, **128**, 2020, paper 161101.

[9] A. MAHMOUD, F. VANDERVEKEN, C. ADELMANN, F. CIUBOTARU, S. COTOFANA and S. HAMDIOUI, *Spin wave normalization toward all magnonic circuits*, IEEE Transactions on Circuits and Systems I: Regular Papers, **68**(1), 2021, pp. 536–549.

[10] A. VAN ZEGBROECK, F. CIUBOTARU, P. ANAGNOSTOU, F. MENG, C. ADELMANN, S. HAMDIOUI AND S. COTOFANA, *Spin wave threshold majority gate*, IEEE 24$^{\text{th}}$ International Conference on Nanotechnology (NANO), Gijon, Spain, 2024, pp. 615–619.

[11] T. FISCHER, M. KEWENIG, D. A. BOZHKO, A. A. SERGA, I. I. SYVOROTKA, F. CIUBOTARU, C. ADELMANN, B. HILLEBRANDS and A. V. CHUMAK, *Experimental prototype of a spin-wave majority gate*, Applied Physics Letters, **110**, 2017, paper 152401.

[12] G. TALMELLI, T. DEVOLDER, N. TRÄGER, J. FÖRSTER, S. WINTZ, M. WEIGAND, H. STOLL, M. HEYNS, G. SCHÜTZ, I. P. RADU, J. GRÄFE, F. CIUBOTARU and C. ADELMANN,*Reconfigurable submicrometer spin-wave majority gate with electrical transducers*, Science Advances, **6**(51), 2022, paper eabb4042.

[13] A. V. CHUMAK, A. SERGA and B. HILLEBRANDS, *Magnon transistor for all-magnon data processing*, Nature Communications, **5**, 2014, paper 4700.

[14] T. BRÄCHER and P. PIRRO, *An analog magnon adder for all-magnonic neurons*, Journal of Applied Physics, **124**, 2018, paper 152119.

[15] A. B. USTINOV, E. LÄHDERANTA, M. INOUE and B. A. KALINIKOS, *Nonlinear spin-wave logic gates*, IEEE Magnetics Letters, **10**, 2019, pp. 1–4, paper 5508204.

[16] A. ROSS, R. LEBRUN, O. GOMONAY, D. A. GRAVE, A. KAY, L. BALDRATI, S. BECKER, A. QAIUMZADEH, C. ULLOA, G. JAKOB, F. KRONAST, J. SINOVA, R. DUINE, A. BRATAAS,

A. ROTHSCHILD and M. KLÄUI, *Propagation length of antiferromagnetic magnons governed by domain configurations*, Nano Letters, **20**, 2019, pp. 306–313.

[17] J. R. HORTENSIUS, D. AFANASIEV, M. MATTHIESEN, R. LEENDERS, R. CITRO, A. V. KIMEL, R. V. MIKHAYLOVSKIY, B. A. IVANOV and A. D. CAVIGLIA, *Coherent spin-wave transport in an antiferromagnet*, Nature Physics, **17**, 2021, pp. 1001–1006.

[18] Á. PAPP, W. POROD and G. CSABA, *Nanoscale neural network using non-linear spin-wave interference*, Nature Communications, **12**, 2021, paper 6422.

[19] J. C. GARTSIDE, K. D. STENNING, A. VANSTONE, H. H. HOLDER, D. M. ARROO, T. DION, F. CARAVELLI, H. KUREBAYASHI and W. R. BRANFORD, *Reconfigurable training and reservoir computing in an artificial spin-vortex ice via spin-wave fingerprinting*, Nature Nanotechnologies, **17**, 2022, pp. 460–469.

[20] D. A. CONNELLY, H. R. O. AQUINO, M. ROBBINS, G. H. BERNSTEIN, A. ORLOV, W. POROD and J. CHISUM, *Complex permittivity of Gadolinium Gallium Garnet from 8.2 to 12.4 GHz*, IEEE Magnetics Letters, **12**, 2021, pp. 1–4, paper 5504504.

[21] A. C. BUNEA, F. CIUBOTARU, F. MENG, C. ADELMANN, O. G. PROFIRESCU and D. NECULOIU, *Investigation of electromagnetic feedthrough in spin wave based majority gates*, International Semiconductor Conference (CAS), Sinaia, Romania, 2024, pp. 101–104.

[22] V. VLAMINCK and M. BAILLEUL, *Spin-wave transduction at the submicrometer scale: Experiment and modeling*, Physical Review B, **81**, 2010, paper 014425.

[23] U. K. BHASKAR, G. TALMELL, F. CIUBOTARU, C. ADELMANN and T. DEVOLDER, *Backward volume vs Damon–Eshbach: A traveling spin wave spectroscopy comparison*, Journal of Applied Physics, **127**, 2020, paper 033902.

[24] F. VANDERVEKEN, V. TYBERKEVYCH, G. TALMELLI, B. SORÉE, F. CIUBOTARU and C. ADELMANN, *Lumped circuit model for inductive antenna spin-wave transducers*, Scientific Reports, **12**, 2022, paper 3796.

[25] R. ERDÉLYI, G. CSABA, L. MAUCHA, F. KOHL, J. GREIL, M. BECHERER, P. PIRRO and A. PAPP, *Design rules for low-insertion-loss magnonic transducers*. Accessed: Mar. 1, 2025. [Online]. Available: https://doi.org/arXiv.2410.14370.

[26] F. BRUCKNER, K. DAVÍDKOVÁ, C. ABERT, A. CHUMAK and D. SUESS, *Micromagnetic simulation and optimization of spin-wave transducers*. Accessed: Mar. 1, 2025. [Online]. Available: http://https://doi.org/10.48550/arXiv.2501.16553.